Published in final edited form as:

Toxicol Pathol. 2022 April ; 50(3): 329–343. doi:10.1177/01926233221089209.

Developing a Solution for Nasal and Olfactory Transport of Nanomaterials

Ryan C. O'Connell[1,2], **Tiana M. Dodd**[1], **Sidney M. Clingerman**[1], **Kara L. Fluharty**[1], **Jayme Coyle**[1], **Todd A. Stueckle**[1], **Dale W. Porter**[1], **Lauren Bowers**[1], **Aleksandr B. Stefaniak**[1], **Alycia K. Knepp**[1], **Raymond Derk**[1], **Michael Wolfarth**[1], **Robert R. Mercer**[1], **Theresa E. Boots**[1], **Krishnan Sriram**[1], **Ann F. Hubbs**[1]

[1]Centers for Disease Control and Prevention, Morgantown, West Virginia, USA

[2]West Virginia University, Morgantown, West Virginia, USA

Abstract

With advances in nanotechnology, engineered nanomaterial applications are a rapidly growing sector of the economy. Some nanomaterials can reach the brain through nose-to-brain transport. This transport creates concern for potential neurotoxicity of insoluble nanomaterials and a need for toxicity screening tests that detect nose-to-brain transport. Such tests can involve intranasal instillation of aqueous suspensions of nanomaterials in dispersion media that limit particle agglomeration. Unfortunately, protein and some elements in existing dispersion media are suboptimal for potential nose-to-brain transport of nanomaterials because olfactory transport has size- and ion-composition requirements. Therefore, we designed a protein-free dispersion media containing phospholipids and amino acids in an isotonic balanced electrolyte solution, a solution for nasal and olfactory transport (SNOT). SNOT disperses hexagonal boron nitride nanomaterials with a peak particle diameter below 100 nm. In addition, multiwalled carbon nanotubes (MWCNTs) in an established dispersion medium, when diluted with SNOT, maintain dispersion with reduced albumin concentration. Using stereomicroscopy and microscopic examination of plastic sections, dextran dyes dispersed in SNOT are demonstrated in the neuroepithelium of the nose and olfactory bulb of B6;129P2-*Omp*^{tm3Mom}/MomJ mice after intranasal instillation in SNOT. These findings support the potential for SNOT to disperse nanomaterials in a manner permitting nose-to-brain transport for neurotoxicity studies.

Corresponding Author: Ann F. Hubbs, Health Effects Laboratory Division, National Institute for Occupational Safety and Health, Centers for Disease Control and Prevention, 1000 Frederick Lane, Morgantown, WV 26508, USA. ahubbs@cdc.gov.

Author Contributions

RO, AH, DP, AS, RM and KS contributed to conception and design; RO, AH and TB drafted the manuscript. All authors contributed to data acquisition, analysis and interpretation. All authors also critically reviewed and revised the manuscript, gave final approval and agreed to be accountable for all aspects of the work.

Authors' Note

The findings and conclusions of this report are those of the author(s) and do not necessarily represent the official position of the National Institute for Occupational Safety and Health, Centers for Disease Control and Prevention.

Declaration of Conflicting Interests

The author(s) declared no potential conflicts of interest with respect to the research, authorship, and/or publication of this article.

Keywords

nanomaterials; nanotoxicology; neurotoxicology; transport mechanisms; dispersion media; nose-to-brain transport; olfactory transport

Introduction

In the early 2000s, the field of material engineering underwent a revolution because of the unique properties of nanomaterials. Not only useful in the material engineering world, nanomaterials promise exciting applications in many fields and technologies. Nanotechnology and nano-enabled products are among the most rapidly growing parts of the economy. Since the first single-walled carbon nanotube (SWCNT) nanodiode was synthesized in 1997, the nanotechnology industry has undergone explosive growth, with the global nanotechnology market valued at $1.0 billion in 2018 and an estimated $2.2 billion in 2025.[1] As a result of this explosive growth, the environmental, health, and safety impacts of many of these materials are not well characterized.[2,3] A relatively new field, nanotoxicology is the study of the health effects of these engineered nanomaterials.[4]

Historically, substances were only evaluated for health effects based on chemical composition and did not take into account the effects of size, shape, and atomic structure on toxicity.[5] Nanoscale dimensions may provide access to biological structures that are inaccessible to larger particles.[5–7] Once a nanomaterial enters the body, the size and shape of the particle also influence where it will travel in the body and how it will interact with cells. High aspect ratio particles such as some types of asbestos fibers or carbon nanotubes have impaired clearance, can puncture cells, cause inflammation, can incorporate themselves into parts of the cell machinery, and interact with intracellular structures including components of the mitotic spindle.[8–13] Both fiber-like and spherical particles have been found in distant target tissues including the brain, liver, lymph nodes, and other internal organs.[14–17] In addition, as particle volume decreases, surface area and the number of particles per unit mass increase.[18] Each time the average size of an object is decreased by half, the surface area of that object increases eight times with respect to its volume. The increase in surface area to volume ratio is critical because surface reactivity of particles plays a major role in their toxicity.[19] Thus, surface area, particle size, interactions with subcellular structures, and the number of particles are all critical in nanotoxicology because they influence the potential adverse interactions of the nanomaterials with targets in the body.[20–22]

Particle interactions in aqueous media can lead to agglomeration or dispersion depending upon components within the media.[23,24] Agglomerated particles often act like larger particles and particle size can affect particle surface area and toxicity, as noted above. Therefore, it is important that dispersion techniques and media for assessing toxicity be developed that can be utilized for a wide variety of nanomaterials. It is also important to tailor the contents of the dispersion media (DM) for a specific target organ. Three common ingredients of a biocompatible DM are an isotonic solution, phospholipids, and proteins. Porter et al.[25] designed a DM that resembles natural lung fluid, based on previous findings that bronchoalveolar lavage fluid,[26] or synthetic lung fluid,[27] provided

excellent nanomaterial dispersion for lung toxicity studies. That DM was developed for pulmonary toxicology studies and disperses nanomaterials of many different shapes and chemical composition.[25] In the DM designed for evaluating pulmonary effects, the protein, mouse albumin, is an important component that may create an artificial protein corona that facilitates the dispersion of the nanomaterials in isotonic phosphate-buffered saline solution.[28] However, once bound in the protein corona, proteins are often resilient and not easily removed.[29] The added size of the protein corona may greatly increase the effective biological size of the nanomaterial.[30] The protein corona could potentially alter toxicity and the growth in size is also a concern due to size limitations for some transport pathways. Specifically, the effective biological size of a nanomaterial with an albumin corona may exceed the 100 nm upper size limit estimated for transport within the central nervous system.[6]

An additional concern is the utilization of phosphate-buffered saline in DM since sodium and phosphate also affect neurons. In particular, neurons transport sodium out of the cell—making high concentrations of sodium undesirable in a medium to evaluate the potential of a particle to be transported within the neuron.[6,17] The sodium concentration of phosphate-buffered saline, 137 mEq/L, is much higher than the sodium concentration of normal human nasal secretions, 34.2 mEq/L.[31] The need to disperse nanomaterials in a balanced electrolyte solution that can be instilled intranasally is important in toxicity studies because some nanomaterials have recently demonstrated the ability to enter the brain through the olfactory pathway from the nose to the brain.[15–17,32–36] The olfactory pathway bypasses the blood-brain barrier because olfactory neurons have direct contact with the lumen of the nose and their first synapse is in the olfactory bulb of the brain. This allows entry into the brain for some particles that cannot cross the blood-brain barrier.[37] To overcome issues with albumin size as well as the effects of sodium and phosphate, we hypothesized that free amino acids, a balanced electrolyte solution, and a mixture of phospholipids could produce a solution that both dispersed nanomaterials and was compatible with neuronal transport.

Our goal was to develop a novel transport media to meet the needs of evaluating nanoscale materials that can be transported from the nose to the brain. The resulting media, SNOT, can disperse nanomaterials and dyes with nanoscale dimensions, enabling intranasal instillation so that potential nose-to-brain transport can be evaluated.

Methods

Animals

B6;129P2-*Omp*^{tm3Mom}/MomJ heterozygous (OMP-GFP) mice were obtained from Jackson Laboratory (Stock #006667) following cryorecovery and were then bred and maintained in an AAALAC-accredited, PHS-assured, environmentally controlled, specific pathogen-free, barrier animal facility. In these mice, green fluorescence protein (GFP) replaces the coding region and a portion of the untranslated region of one copy of the olfactory marker protein gene (OMP). These mice display intense green fluorescence in olfactory neurons from the nose to their axonal terminus in glomeruli of the olfactory bulb.[38] Wild-type controls were from this colony. A Qiagen DNeasy blood and tissue kit was used for DNA isolation, and gel electrophoresis was used to identify genotypes by polymerase chain reaction (PCR) using

procedures from the mouse supplier. To reduce the use of animals in this study and because preliminary data were from male mice, all mice used for experimental purposes in this study were male. All procedures were reviewed and approved by the CDC-Morgantown Animal Care and Use Committee.

Chemicals

1,2-Dimyristoyl-sn-glycero-3-phosphocholine (DMPC) was acquired from Sigma-Aldrich (St Louis, MO, product #P2663). 1,2-Dipalmitoyl-sn-glycero-3-phosphocholine (DPPC) was acquired from Sigma-Aldrich (St Louis, MO, product #P0763). Lactated Ringer's solution (LRS) was acquired from Patterson Veterinary (Greeley, CO, catalog #078696319). Dulbecco's phosphate-buffered saline (PBS) without calcium chloride or magnesium chloride was from Sigma-Aldrich (St Louis, MO, catalog #D8537). TrophAmine 10% amino acid solution was acquired from Medline Industries (Northfield, IL, catalog #BMGS9341H). Ethanol was acquired from Sigma-Aldrich (St Louis, MO, catalog #E7023–500ml). Mouse albumin was acquired from Innovative Research (Novi, MI, catalog #IRMSA) and tested free of common murine pathogens (IDEXX, IMPACT 1 PCR Panel). Hexagonal boron nitride (HBN) was acquired from Sky Spring Nanomaterials, Inc (Houston, TX). Tetramethylrhodamine anionic lysine-fixable dextran (rhodamine dextran, 3000 MW, catalog #D3308) and Alexa Fluor 680 anionic dextran (3000 MW, catalog #D34681) were acquired from ThermoFisher (Waltham, MA).

Composition and Preparation of SNOT

The SNOT is composed of 1 mg/mL DPPC (as 10 μL of a 1:10 dilution of DPPC in 200 proof ethanol), 0.25 mg/mL DMPC (as 25 μL of a 1:100 dilution of DPPC in 200 proof ethanol), 959 μL/mL LRS and 6 μL/mL TrophAmine. Each was added in that order to a 2 mL tube; the addition of TrophAmine directly to DPPC caused irreversible gel formation. Chemicals were kept at 37°C and the solution was vortexed as each ingredient was added. Finally, the solution was vortexed for 1 minute to thoroughly dissolve all components when additions were completed. The solution was made fresh for each experiment.

Calculation of SNOT Density, Viscosity, and Refractive Index

SNOT was pre-equilibrated to 37°C, dispensed into a tared 10 mL volumetric flask and placed into an analytical balance for gravimetric density determination. For viscosity measurement, SNOT temperature was equilibrated to approximately 25°C before loading into a size 25 Cannon-Fenske Routine viscometer (Cannon Instruments: State College, PA) and then submerged in a 37°C bath for a minimum of 10 minutes before measurement. The efflux time was measured in quadruplicate in seconds and converted to the dynamic viscosity using efflux time, SNOT density, and the viscometer-specific constant (0.0020625 centiStokes/second). The SNOT refractive index was measured via an ISO-9001 certified hand-held refractometer according to the manufacturer's instructions (Reichert Analytical Instruments; Dewpew, NW; Catalog #AR200).

Sonication of Nanomaterials in SNOT

Because of the variations between sonicators, the delivered acoustic power (P) of the sonication equipment (Sonics Vibra Cell, Model VC505 with 2.75 in cup horn, Newton, CT) was calculated to be 3.34Js^{-1} using published methods.[39]

$$(P) \times (t)/(V) = DSE,$$

where P is the acoustic power (J/s), t is time (seconds), V is volume (mL), and DSE is delivered sonication energy (J/mL).

Unless specified, 5 mL solutions were sonicated for 1 minute to achieve 40 J/mL delivered sonication energy (DSE) followed by 1 minute of rest. This was repeated 5 times for a total of 200 J/mL DSE.

Dynamic Light Scattering

Dynamic light scattering (DLS) measurements (Zetasizer Nano ZS, Model Zen3600, Malvern) were used to determine particle hydrodynamic diameter (dH) throughout the study. Sample physical properties for DLS measurements, that is, density, refractive index, and viscosity, were calculated for SNOT. Refractive index and absorption values for HBN were obtained from literature (Table 1).[40,41] For DLS measurements, a sample volume of 0.5 mL was placed in low volume cuvettes (Zetasizer, ZEN0040; Malvern, United Kingdom). Number distributions were collected and averaged with five replicates. After sonication, dispersed nanomaterials were placed in a water bath at 37°C.

Intranasal Exposures in Mice

Mice were anesthetized using isoflurane anesthesia with induction in a bell jar and maintenance of anesthesia with a SomnoSuite low-flow anesthesia system (Kent Scientific, Torrington, CT). SNOT or dyes dispersed in SNOT were used for intranasal instillation with modification of a previously described procedure.[42–44] Briefly, the solution was vortexed for approximately 1 minute and 20 microliters were administered intranasally. For intranasal administration, the mouse was placed in sternal recumbency and when surgical plane anesthesia was achieved, the mouse was rotated away from the anesthesia nose cone and a drop of SNOT solution at the end of a sterile micropipette tip was placed in front of one nostril so that normal respiration drew the drop into the nose of the mouse; a second drop was then placed at the end of the micropipette tip in front of the other nostril. When the second drop was inspired, the mouse was rotated back to the nose cone to breathe anesthetic for approximately 30 seconds and then the procedure was repeated until the entire 20 µL was inspired. Anesthesia continued for approximately 45 seconds following the final inspiration. To prevent aspiration of bedding, mice recovered from anesthesia in a recovery cage lined with absorbent laboratory paper and were transferred back to their home cage when ambulatory.

Pharyngeal Aspiration Exposures in Mice

Lungs of two mice were exposed to SNOT using a previously described pharyngeal aspiration procedure.[45]

Intranasal Exposures to Dextran Dyes

While not typically considered nanomaterials, dextrans are polysaccharides of low toxicity, hydrophilic, and available as conjugates of several dyes. These conjugates are typically between 3000 and 70,000 Daltons, which corresponds to an approximate size of 1 to 20 nm. Some dextran dyes can be up to 2,000,000 Daltons in mass. A 3000 Dalton dextran has a diameter of approximately 2.48 nm.[46] We used 3000 Dalton dextran dyes to track the potential for a nanoscale particle to enter the olfactory bulb after intranasal administration in SNOT because they previously have been shown to undergo neuronal transport in many different conditions, including after intranasal administration in rats.[47]

A 0.5% concentration solution of dextran dye suspended in SNOT was administered to OMP-GFP mice through intranasal instillation as described above. Rhodamine dextran (tetramethylrhodamine 3000 MW anionic lysine-fixable dextran) and anionic near-infrared (NIR) dextran in SNOT (Alexa Fluor 680; 3000 MW, Anionic) were used to track the movement of dextran in SNOT in the nasal cavity and olfactory bulb using stereomicroscopy and epifluorescence.

Stereomicroscopy

Mice were euthanized by an overdose of sodium pentobarbital-containing euthanasia solution. The dorsal portion of the neurocranium was removed and the olfactory bulb and cerebrum were examined using an Olympus SZX16 research stereomicroscope and photographed using a DP73 cooled digital camera or an Olympus XM10-IR microscope camera. The nose and brain were then immersion-fixed in 10% neutral buffered formalin.

Histopathology

Tissues were fixed in neutral buffered formalin. Noses were decalcified in 13% formic acid and cross-sections were taken at four levels. The four levels of the mouse nose were from the three standard trimming locations[48] with an additional level just behind the third standard location. The fourth level was included because it usually contains more olfactory nerve fibers crossing the cribriform plate than the standard sections. Tissues were processed in a Thermo Scientific Excelsior AS tissue processor. Hematoxylin and eosin–stained sections of lung and nose were evaluated by a board-certified veterinary pathologist.

Plastic Sections

Plastic sections were used to confirm entry of rhodamine dextran into the neuroepithelium of the nose. Lysine fixable dextran dyes are preserved with aldehyde fixatives such as formalin, but the fluorescence is lost in paraffin-embedded tissue sections. However, the fluorescence of aldehyde fixable dyes can be visualized in unstained plastic tissue sections.[47] Therefore, sections of level T2 of the nose from nine mice exposed to rhodamine dextran in SNOT and two mice exposed to SNOT alone were embedded in plastic using a JB-4 plastic embedding kit as previously described.[49] Suitable-oriented dextran-exposed samples were obtained and photographed from the following time points: 3 hours (n = 2), 6 hours (n = 2), 1 day (n = 3), and 1 week after exposure (n = 1). Plastic sections with adequate orientation from mice exposed to SNOT alone were obtained and photographed from the following time points: 3 hours (n = 1) and 1 week (n = 1) after exposure.

Estimation of Median Diameter From DLS Data

The median of particle diameter was estimated for DLS measurement of particle size because particle diameter distributions tend to be skewed by a small fraction of large particles, thus the median is a better measure of center of the particle diameter distribution than is the mean. In addition, in the nose, large particles can simply be expelled out of the nose with a sneeze or a snort. Conversely, having a large portion of particles small enough to undergo olfactory transport is important in evaluating potential nose-to-brain transport. To estimate the median particle diameter for each DLS data set, the discrete diameter measurements from DLS were repeated to create a new data set comprising the discrete diameter measurements proportional to their average percentage across the trials (rounded up to the next integer). For example, the vesicle diameter measured 32.67 nm was on average 20.39% of the vortexed SNOT, so the newly created data set for vortexed SNOT sample contained the value 32.67 repeated 21 times. A Wilcoxon rank sum test was then used on each new data set to estimate a (pseudo) median value along with corresponding 95% confidence intervals via the approximation method. To estimate the 1st percentile of each data set, a function was approximated from the original distribution of discrete diameter measurements and used to integrate from the lowest diameter measurement to the 1st percentile. All analyses were conducted using R (v 3.6.0) in RStudio (Vienna, Austria).

Results

SNOT Is an Isotonic, Balanced Electrolyte Solution Containing Amino Acids and Two Phospholipids

In preliminary studies, PBS was replaced with LRS in the existing DM developed for lung exposures. This solution dispersed a test nanomaterial, HBN. However, simply replacing albumin with a comparable amount of balanced amino acids in the modified DM created a solution that failed to fully disperse nanomaterials. A previous study demonstrated that a solution containing 150 μL/mL Survanta could disperse nanomaterials.[27] Since Survanta has 25 mg/mL phospholipids of which 74.9 ± 5% is reported to be DPPC,[50] we next tried much higher concentrations of DPPC. However, a solid (gel) precipitate formed at DPPC concentrations of 1.27 or 2.25 mg/mL at room temperature, indicating that the solution had transitioned from the liquid to the solid (gel) state. The liquid/solid transition of phospholipid solutions is affected by multiple factors, including the type of phospholipid, the phospholipid concentration, the presence of proteins, and temperature of the solution.[51–53] At 37°C in the presence TrophAmine (an amino acid solution), no gel formed with a DPPC concentration of 0.63 mg/mL or with a concentration of 1.01 mg/mL DPPC and 0.25 mg/mL DMPC, another phospholipid that transitions to a solid at a lower temperature than DPPC. Therefore, the phospholipids in SNOT are 1 mg/mL DPPC and 0.25 mg/ml DMPC. At 37°C, SNOT was prepared by either vortexing or probe sonication for 1 minute at 20% amplitude (calculated to deliver 3.34 J/s).

Parameters for Measurement of DLS

DLS measurements were used to determine particle size throughout the study. To make accurate measurements, the density, refractive index, and viscosity were calculated for SNOT and the density and refractive index were calculated for HBN (Table 1).

Optimization of Sonication Procedures to Disperse Nanomaterials in SNOT

HBN was selected for evaluation because it is used in scenarios where aerosols are easily generated, yet HBN is insoluble in water and tends to agglomerate in solution. Potential aerosol generating procedures using HBN nanomaterials include use as lubricants for functions including mechanical lubrication and the coating of bullets.[54–56] The SNOT colloidal suspensions were either vortexed or sonicated under varying conditions (Figure 1A, Table 2) with intermittent rest periods of 1 minute to create test suspensions.[57] Then suspensions containing SNOT and HBN were sonicated in probe and cup sonicators at various time points and intensities, and the diameter of the resulting colloidal solutions was analyzed with DLS [Figure 1B, Table 3). SNOT alone (without HBN) contained particles, presumed to be micelles and microvesicles of DPPC and DMPC, with a median 35 nm in diameter (Table 3). For HBN in SNOT, the number of nanomaterials under 100 nm increased with increasing sonication time, consistent with greater nanomaterial dispersion and fewer agglomerates up to five sonications. After an optimal dispersion is reached with five 1-minute cup sonications with a 1-minute rest period between each sonication, nanomaterial size increased with more sonication (Figure 1B), which indicated agglomeration from higher energy input. This is evidenced by the presence of particles larger than ~100 nm after more than five sonications. The median particle size after optimal dispersion with five sonications was determined to be 43.8 nm (Table 3).

Polarized Light Microscopy Confirms HBN Dispersion in SNOT

Light microscopy examination of HBN dispersed in SNOT demonstrated nanomaterials with few visible agglomerates that were birefringent in polarized light (Figure 2).

Dextran Conjugated Dyes in SNOT Enter the Olfactory Neuroepithelium and Reach the Olfactory Bulb of the Brain

Whole-brain epifluorescence stereomicroscopy documented red fluorescence in nasal passages of mice exposed to rhodamine dextran in SNOT (Figure 3, Table 4).

To determine whether the rhodamine dextran was entering into the neuroepithelium of the nose and the olfactory bulb, additional mice were exposed to 0.5% rhodamine dextran and sacrificed at 3 hours, 6 hours, 1 day, or 1 week after exposure (n = 3 per time point) or exposed to SNOT alone and sacrificed at 3 hours or 1 week after exposure (n = 3). Fluorescence microscopy of formalin-fixed, decalcified plastic sections from the mice exposed to rhodamine dextran in SNOT demonstrated punctate red fluorescence consistent with rhodamine dextran in the neuroepithelium at 3 hours (n = 2), 6 hours (n = 2) and 1 day (n = 3) after exposure (Figure 4). Punctate red fluorescence was also identified in the neuroepithelium of one mouse 1 week after exposure (n = 2, Figure 5) and was not seen in mice exposed to SNOT alone at 3 hours (n = 1) and 1 week (n = 1) after exposure. Red and green fluorescence was visualized in plastic sections of the olfactory bulb from rhodamine dextran-exposed mice (n = 3) but was also seen in the olfactory bulb of control (SNOT-exposed) mice (n = 3). The red fluorescence in the olfactory bulb of control mice and some of the red fluorescence in the rhodamine dextran-exposed mice were consistent with the granular autofluorescence of lipofuscin, as previously described in the olfactory bulb of unexposed young mice.[58] Because red fluorescence due to lipofuscin could not

clearly be distinguished from red fluorescence due to rhodamine dextran, this prevented definitive identification of the rhodamine dextran in plastic sections of the olfactory bulb from mice exposed to dextran dye in SNOT.

Therefore, to demonstrate the movement of SNOT into the olfactory bulb, it was necessary to use a dextran dye with emissions in the near-infrared (NIR) because of the low background emissions and greater tissue penetration of NIR fluorescence.[59,60] Mice were exposed intranasally to 0.5% anionic NIR dextran (Alexa Fluor 680; 3000 MW, Anionic) in SNOT. NIR fluorescence was demonstrated in the nose and olfactory bulb by NIR epifluorescence stereomicroscopy as early as 15 minutes following intranasal instillation (Table 5, Figure 6). However, the NIR dextran was not lysine fixable and was not visible in plastic sections.

No Morphologic Alterations Associated With SNOT Instillation Were Found in the Mouse Nose

No exposure-related morphologic alterations were detected in sections of noses 1 hour after intranasal instillation of SNOT (n = 3, Figure 7). Similarly, in the dextran dye studies where exposure of the nose was documented by epifluorescence stereomicroscopy, rhodamine dextran (0.5%), NIR dextran (0.5%), and SNOT alone caused no exposure-related changes in the histopathology of the nose of intranasally instilled mice at 1 hour, 3 hours, 6 hours, or 1 day after exposure (Table 6).

Following the pharyngeal aspiration of SNOT, a basophilic film resembling a thick mucus layer lined some bronchioles in one of two exposed mice (Figure 8). However, mucous-producing cells are rare or absent in airways distal to the trachea in normal unexposed mice.[61] The associated airway epithelium was morphologically normal without evidence of mucous metaplasia suggesting the material could be persistent SNOT. Due to the potential persistence of SNOT in bronchioles, no additional mice were exposed by pharyngeal aspiration during this study.

Development of a Two-Step Process for Optimal Dispersion of Fiber-Like Nanomaterials

The established DM for respiratory instillation studies disperses a spectrum of nanomaterials including high aspect ratio particles such as multiwalled carbon nanotubes (MWCNTs). It is composed of PBS with 0.6 mg/mL mouse serum albumin and 10 μg/mL DPPC, with or without 5.5 mM D-glucose.[25,62] However, in initial experiments, a well-characterized MWCNT material, Mitsui-7, produced a precipitate when sonicated in SNOT. In addition, as mentioned earlier, we were concerned about (1) PBS and particularly the sodium in the established DM due to potential interference with olfactory transport and (2) the effect of albumin on the size of nanomaterials. Therefore, we first replaced PBS with LRS in established DM to create a modified DM. MWCNTs at 0.95 mg/mL were sonicated five times for 1 minute followed by a dilution to a concentration of 0.1 mg/mL in either established DM modified to contain LRS in place of PBS (Figure 9A) or SNOT (Figure 9B). The MWCNTs remained well dispersed under both conditions as assessed by both microscopy and DLS. Furthermore, DLS indicated a reduction in the calculated diameter of MWCNTs in the SNOT mixture compared with the MWCNTs in standard DM (Figure 9C).

Thus, a two-step procedure, using initial dispersion in established DM modified to contain LRS, followed by a dilution in SNOT can reduce the albumin, phosphate, and sodium concentration and disperse MWCNTs.

Discussion

We hypothesized that free amino acids, a balanced electrolyte solution, and a mixture of phospholipids could produce a biocompatible solution that both dispersed nanomaterials and was compatible with neuronal transport. Our findings support that hypothesis. We began by considering existing biocompatible dispersion media, then modifying the phospholipid composition and concentration, and added free amino acids to LRS, a balanced electrolyte solution. This mixture created a protein-free solution compatible with neuronal transport that disperses nanoscale dyes and some insoluble nanomaterials.

Short-term toxicity tests for screening potentially hazardous particles often involve instillation of aqueous suspensions of the test particles. However, particles tend to agglomerate when suspended in aqueous solution. Since insoluble nanomaterials can be aerosolized as individual particles but agglomerate in aqueous media, toxicity testing of such nanomaterials should include evaluations of dispersed nanomaterials. The toxicity of dispersed nanomaterials can be distinct from the toxicity of the same nanomaterials when agglomerated.[63] The toxicity of nanomaterial agglomerates is often comparable to that of particles the size of the agglomerates.[5,6,22,64] This comparable toxicity is because the toxicity of poorly soluble particles usually increases with increasing surface area per unit mass—and surface area per unit mass greatly increases in the nanoscale while decreasing in their agglomerates.[65,66] In addition, toxicity can sometimes be enhanced when nanoscale particles have access to biological structures inaccessible to larger particles. In the case of neurotoxicity studies, the theoretical maximum size for neuronal transport of an insoluble nanomaterial is approximately 100 nm.[6] Thus, media for nanomaterial neurotoxicity studies should disperse the nanomaterials in aqueous solution while avoiding changes in biological size potentially caused by interactions with components, such as proteins, in the dispersion media.

Some aerosolized nanomaterials can be inhaled and enter the brain through nose-to-brain transport, resulting in concern for potential neurotoxicity. Thus, the dispersion of nanomaterials within biocompatible aqueous liquids is essential to evaluating the toxicity of such nanomaterials in short-term toxicology studies.[34,67] Dispersion media for such studies have similarities to some drug delivery systems developed for nose-to-brain transport of pharmaceuticals, which is an area of active research.[68–71] For short-term testing of neurotoxicity of occupational and environment nanoparticles using intranasal instillation, dispersion solutions, like pharmaceutical drug delivery systems, should be both biocompatible and compatible with olfactory transport. However, unlike many nose-to-brain drug delivery systems, the nanomaterials evaluated in occupational and environmental toxicology studies are not intentionally designed to target the brain. Using knowledge of protein coronas, the properties of phospholipids, and the components of natural fluid in the nose, we developed a balanced electrolyte solution that indeed dispersed nanomaterials that we evaluated. Viscosity measurements of SNOT were below 1 cP, which confirmed the

surfactant properties of the solution. The capacity of SNOT to disperse nanomaterials was examined using by DLS and microscopy with HBN as the test nanomaterial. In addition, the capability of SNOT to use nose-to-brain transport for delivery to the brain was determined by the instillation of nanoscale dextran dyes in the OMP-GFP mouse, a transgenic mouse model with fluorescent olfactory neurons.

There are two important roles phospholipids play in dispersion media. First, they increase the hydrophilicity of nanomaterials. Second, they tailor the viscosity of the medium to closely match the secretions of the organ. Phospholipids are amphiphilic, containing a nonpolar end and a polar end. Phospholipids have been found to attach themselves by their nonpolar ends to carbon nanotubes, leaving the polar, hydrophilic part of the phospholipid to interact with the aqueous solution, and increasing dispersion.[72–74] In addition, phospholipids such as DMPC and DPPC, being main components of the plasma membrane in cells, spontaneously form micelles and bilayer vesicles, in which nonpolar, hydrophobic nanomaterials can stably suspend.[52,75,76] The introduction of phospholipids can also facilitate the cellular internalization of nanomaterials, while the ratio of phospholipid types can adjust the viscosity of the media and rate of micelle/vesicle fusion and activity at body temperature.[76–78]

The existing DM, a medium commonly used for pulmonary toxicity studies, contains low concentrations of the major phospholipid in natural surfactant, DPPC, and contains a protein, mouse albumin.[25] The albumin may replace functions of proteins in natural surfactant, which is also an excellent dispersing agent.[26] Indeed, proteins contribute to the functional properties of surfactant in the lung.[79,80] These properties include reducing surface tension, increasing vesicular fusion activity, and broadening the temperature range for transition from a liquid to a solid state.[52,79–82] In designing a protein-free dispersion medium for the nose, we needed to maintain those properties. We increased the concentration of DPPC relative to the existing DM to increase the dispersion capabilities in the absence of protein. Combining DPPC with another phospholipid, such as DMPC, changes the surfactant properties of the solution in ways that somewhat mimic the effects of protein, especially at physiological temperatures. We added DMPC to broaden and raise the temperature of phospholipid transition from a gel to a liquid state so that the transition temperature was close to body temperature.[52] Natural surfactant has a broad gel to liquid transition temperature range.[52] We used DMPC to enhance surface activity functions that are associated with the broadened transition temperature normally created by surfactant proteins. Consistent with previous studies showing that phospholipids appear to enhance nanomaterial dispersal and mixtures of phospholipids alter the temperature of gel formation,[27,52] HBN in SNOT remained dispersed in an aqueous solution that is near gel-sol transition at body temperature.

In dispersion solutions, proteins can play another role because they can adsorb and surround nanomaterials where they form a surface coating known as the corona.[83] The makeup of the protein corona has effects on toxicity while allowing individual nanomaterials or small agglomerates to stay dispersed for extended time periods in aqueous solutions.[28,29] For example, albumin in the established DM can be a concern if it has the potential for biological effects that could affect the outcomes of some studies.[84] In addition, albumin

is isolated from mice and can be contaminated with murine pathogens and bacterial endotoxin.[85] Testing of albumin for murine pathogens is an expensive, time-consuming process and animal facility disease outbreaks have been associated with use of biologics, even when tested for murine pathogens.[85] A potential substitute for albumin is to use Survanta, a modified bovine surfactant extract used to treat respiratory distress syndrome in premature infants.[27,86] We decided not to replace albumin with Survanta because it contains a modified bovine surfactant with bovine protein which could potentially cause an immune response in mice. Instead, we replaced albumin with TrophAmine, an amino acid solution typically used to deliver amino acids intravenously in infants.[87] Importantly, the absence of any animal proteins means SNOT is compatible with different species.

DLS is a technique commonly used to characterize the size of nanomaterials dispersed in solution. Typically, the most important parameters measured are the volume data, which indicates the size of nanomaterials with respect to the percentage of volume that they make up in the solution. In addition, zeta potential, which is an indirect measure of particle surface charge, is an indicator of the stability of nanomaterials in suspension. An additional important measurement, the polydispersity index (PDI), provides an indicator of the heterogeneity of nanomaterial size. Since SNOT contains phospholipid nanomaterials (vesicles, microvesicles, and micelles), nanomaterial suspensions in SNOT are intrinsically somewhat polydisperse suspensions. PDI is a useful indicator of the appropriateness of algorithms used to calculate particle size from DLS measurements; generally, cumulants analysis is most appropriate when the PDI is < 0.2 but can also be useful when PDI values are in the range of 0.1 to 0.7.[88] Based on PDI values, the DLS calculations of particle size in our study are useful for evaluating nanomaterial sizes relative to critical biological targets, but should not be viewed as precise measurements. In this particular study, we are interested in maximizing the number of particles under the 100 nm theoretical limit for olfactory transport.[6] Therefore, the number data was the most important parameter for our research. Indeed, the diameter of the majority of HBN nanoparticles dispersed in SNOT was well below 100 nm.

Surprisingly, although SNOT was able to disperse HBN and nanoscale dextran dyes, MWCNTs were not well dispersed by SNOT alone. To determine if it was possible to dilute DM containing MWCNTs in SNOT to minimize the potential effects of albumin, we modified the established DM by replacing PBS with LRS. We observed no significant changes in the size of MWCNTs dispersed in DM made with LRS compared with DM made with PBS. When MWCNTs were dispersed in modified DM made with LRS and then diluted in SNOT, DLS demonstrated a decrease in the average hydrodynamic diameter of the particles in the SNOT relative to the size of the particles in modified DM. This change in size suggests a decreased association of albumin with MWCNT when the suspension is diluted in SNOT. Unfortunately, the association of proteins such as albumin with the surface of nanomaterials to create a protein corona cannot be seen by light microscopy or standard electron microscopy procedures.[89] An important limitation of using DLS to measure hydrodynamic diameter is that DLS is designed to analyze suspensions of spherical nanomaterials.[90] MWCNTs are high aspect ratio nanomaterials, not spheres. However, DLS measurements of high aspect ratio nanomaterials can be corrected if additional factors are known.[91] DLS measurements, therefore, have value for demonstrating the reduction in

size of the same particle in two different dispersion media. To confirm the dispersion of MWCNTs in DM and then further diluted with SNOT, we visually compared the samples utilizing microscopy. The MWCNTs diluted in SNOT remained well dispersed. Thus, this two-step procedure for dispersing MWCNT replaces PBS with LRS and reduces the amount of albumin with corresponding apparent decrease in MWCNT particle size.

We were able to demonstrate the movement of SNOT into unfixed olfactory bulbs by the combined use of GFP-OMP mice and stereomicroscopy using epifluorescence of an NIR-emitting dye. The mice have a gene for green fluorescent protein replacing a portion of the 3' region of olfactory marker protein gene. Olfactory marker protein is specifically expressed in olfactory neurons. While the cell bodies of the olfactory neurons are in the olfactory neuroepithelium of the nose, the axons of the olfactory neurons traverse the cribriform plate and synapse in the glomeruli of the olfactory bulb.[38,92] This marker, therefore, allows us to use epifluorescence stereomicroscopy to demonstrate NIR dye and GFP colocalization when the NIR dye is in intracranial axons of olfactory neurons in the GFP-OMP mouse.

Rhodamine dextran dye in SNOT provided converging lines of evidence that SNOT could carry dextran dye into the olfactory neuroepithelium because it is lysine-fixable and could be demonstrated in plastic sections. While the fluorescent probes conjugated to rhodamine dextran were visible and could be detected in plastic sections, autofluorescence of lipofuscin was also detected in the rhodamine channel in the olfactory bulb but not the neuroepithelium of the nose. For this reason, we also imaged with NIR dextran, which allowed direct demonstration of NIR dextran in the olfactory bulb itself by stereomicroscopy of unfixed tissue as noted above. The use of GFP-OMP mice in conjunction with stereomicroscopy allowed the NIR fluorescence to be localized to the region of the olfactory bulb containing the axons of olfactory neurons. In plastic sections, colocalization of lysine-fixable rhodamine dextran with neurons in the neuroepithelium of the nose was confirmed through plastic-embedded sections. The presence of rhodamine dextran in the olfactory neuroepithelium, combined with the presence of NIR dextran in the olfactory bulb of GFP-OMP mice, provides strong and converging lines of evidence demonstrating that nanoscale materials dispersed in SNOT were transported from the nose, through the olfactory neuroepithelium, to the olfactory bulb. This demonstration enables evaluating the potential for nose-to-brain of other nanomaterials that are well dispersed in SNOT.

In summary, the findings support our hypothesis that SNOT is biocompatible, compatible for intranasal instillation, disperses some nanomaterials, and allows for the study of potential nose-to-brain transport. We found that SNOT disperses insoluble HBN nanomaterials. In addition, when used to dilute MWCNT dispersion that was initiated with established DM, SNOT maintained and optimized the dispersion of the nanotubes while lowering concentrations of albumin. In addition, nanoscale dextran dispersed in SNOT was delivered from the nose to the olfactory bulb in the mouse. Future research needs to be done to demonstrate the uptake of other nanomaterials into the brain with SNOT to elucidate nose-to-brain transport pathways and potential neurotoxicity of nanomaterials or the use of nanomaterials in facilitating drug delivery.

Acknowledgment

We are grateful to Diana Richardson for preparation of tissue sections for microscopic evaluation.

Funding

The author(s) disclosed receipt of the following financial support for the research, authorship, and/or publication of this article: Funding for this study was from the intramural Nanotechnology Research Center Project: *Nanoparticle-induced Neuropathology* 6939051B.

References

1. Allied Market Research. Nanotechnology market by type (nanodevices and nanosensors) and application (electronics, energy, chemical manufacturing, aerospace & defense, healthcare, and others): global opportunity analysis and industry forecast, 2018–2025. Published 2019. Accessed March 19, 2022. https://www.marketresearch.com/Allied-Market-Research-v4029/Nanotechnology-Type-Nanodevices-Nanosensors-Application-12552012/.
2. National Research Council. Research Progress on Environmental, Health, and Safety Aspects of Engineered Nanomaterials. Washington, DC: National Academies Press; 2013.
3. Collier ZA, Kennedy AJ, Poda AR, et al. Tiered guidance for risk-informed environmental health and safety testing of nanotechnologies. J Nanopart Res. 2015;17(3):1–21.
4. Marquis BJ, Love SA, Braun KL, Haynes CL. Analytical methods to assess nanoparticle toxicity. Analyst. 2009;134(3):425–439. doi:10.1039/b818082b. [PubMed: 19238274]
5. Hubbs A, Porter D, Mercer R, Castranova V, Sargent L, Sriram K. Nanoparticulates. In: Haschek WM, Rousseaux CG, Wallig MA, Bolon B, Ochoa R, eds. Haschek and Rousseaux's Handbook of Toxicologic Pathology. 3rd ed. Waltham, MA: Elsevier/AP; 2013:1373–1419.
6. Patchin ES, Anderson DS, Silva RM, et al. Size-dependent deposition, translocation, and microglial activation of inhaled silver nanoparticles in the rodent nose and brain. Environ Health Perspect. 2016;124(12):1870–1875. [PubMed: 27152509]
7. Nance EA, Woodworth GF, Sailor KA, et al. A dense poly (ethylene glycol) coating improves penetration of large polymeric nanoparticles within brain tissue. Sci Transl Med. 2012;4(149):149ra119.
8. Morgan A, Talbot R, Holmes A. Significance of fibre length in the clearance of asbestos fibres from the lung. Occup Environ Med. 1978;35(2):146–153.
9. Donaldson K, Murphy F, Schinwald A, Duffin R, Poland CA. Identifying the pulmonary hazard of high aspect ratio nanoparticles to enable their safety-by-design. Nanomedicine. 2011;6(1):143–156. [PubMed: 21182425]
10. Sargent LM, Shvedova AA, Hubbs AF, et al. Induction of aneuploidy by single-walled carbon nanotubes. Environ Mol Mutagen. 2009;50(8):708–717. doi:10.1002/em.20529. [PubMed: 19774611]
11. Sargent LM, Hubbs AF, Young SH, et al. Single-walled carbon nanotube-induced mitotic disruption. Mutat Res. 2012;745(1–2):28–37. [PubMed: 22178868]
12. Hubbs AF, Mercer RR, Benkovic SA, et al. Nanotoxicology—a pathologist's perspective. Toxicol Pathol. 2011;39(2):301–324. [PubMed: 21422259]
13. Archer VE. Carcinogenicity of fibers and films: a theory. Med Hypotheses. 1979;5(11):1257–1262. [PubMed: 231733]
14. Liu Q, Shen Y, Chen J, et al. Nose-to-brain transport pathways of wheat germ agglutinin conjugated PEG-PLA nanoparticles. Pharm Res. 2012;29(2):546–558. [PubMed: 22167350]
15. Kao YY, Cheng TJ, Yang DM, Wang CT, Chiung YM, Liu PS. Demonstration of an olfactory bulb-brain translocation pathway for ZnO nanoparticles in rodent cells in vitro and in vivo. J Mol Neurosci. 2012;48(2):464–471. [PubMed: 22528453]
16. Shah L, Yadav S, Amiji M. Nanotechnology for CNS delivery of bio-therapeutic agents. Drug Deliv Transl Res. 2013;3(4):336–351. [PubMed: 23894728]
17. Mistry A, Stolnik S, Illum L. Nanoparticles for direct nose-to-brain delivery of drugs. Int J Pharm. 2009;379(1):146–157. [PubMed: 19555750]

18. National Nanotechnology Initiative. What's so special about the nanoscale? Date unknown. Accessed March 19, 2022. https://www.nano.gov/nanotech-101/special.
19. Hubbs AF, Sargent LM, Porter DW, et al. Nanotechnology: toxicologic pathology. Toxicol Pathol. 2013;41(2):395–409. [PubMed: 23389777]
20. Schmid O, Stoeger T. Surface area is the biologically most effective dose metric for acute nanoparticle toxicity in the lung. J Aerosol Sci. 2016;99:133–143.
21. Kreyling WG, Semmler-Behnke M, Möller W. Ultrafine particle-lung interactions: does size matter? J Aerosol Med. 2006;19(1):74–83. [PubMed: 16551218]
22. Gliga AR, Skoglund S, Wallinder IO, Fadeel B, Karlsson HL. Size-dependent cytotoxicity of silver nanoparticles in human lung cells: the role of cellular uptake, agglomeration and Ag release. Part Fibre Toxicol. 2014;11(1):1–17. [PubMed: 24382024]
23. Hartmann NB, Jensen KA, Baun A, et al. Techniques and protocols for dispersing nanoparticle powders in aqueous media—is there a rationale for harmonization? J Toxicol Environ Health B Crit Rev. 2015;18(6):299–326. [PubMed: 26397955]
24. Luchini A, Vitiello G. Understanding the nano-bio interfaces: lipid-coatings for inorganic nanoparticles as promising strategy for biomedical applications. Front Chem. 2019;7:343. [PubMed: 31165058]
25. Porter D, Sriram K, Wolfarth M, et al. A biocompatible medium for nanoparticle dispersion. Nanotoxicology. 2008;2(3):144–154.
26. Sager TM, Porter DW, Robinson VA, Lindsley WG, Schwegler-Berry DE, Castranova V. Improved method to disperse nanoparticles for in vitro and in vivo investigation of toxicity. Nanotoxicology. 2007;1(2):118–129.
27. Wang L, Castranova V, Mishra A, et al. Dispersion of single-walled carbon nanotubes by a natural lung surfactant for pulmonary in vitro and in vivo toxicity studies. Part Fibre Toxicol. 2010;7:31. [PubMed: 20958985]
28. Del Pino P, Pelaz B, Zhang Q, Maffre P, Nienhaus GU, Parak WJ. Protein corona formation around nanoparticles—from the past to the future. Mater Horiz. 2014;1(3):301–313.
29. Monopoli MP, Walczyk D, Campbell A, et al. Physical-chemical aspects of protein corona: relevance to in vitro and in vivo biological impacts of nanoparticles. J Am Chem Soc. 2011;133(8):2525–2534. [PubMed: 21288025]
30. Casals E, Pfaller T, Duschl A, Oostingh GJ, Puntes V. Time evolution of the nanoparticle protein corona. ACS Nano. 2010;4(7):3623–3632. [PubMed: 20553005]
31. Sakakura Y, Majima Y, Yoshii S, Taniguchi T, Miyoshi Y, Ohyama M. Nasal secretion from normal subjects. Auris Nasus Larynx. 1979;6(2):71–78. [PubMed: 45174]
32. Hopkins LE, Laing EA, Peake JL, et al. Repeated iron-soot exposure and nose-to-brain transport of inhaled ultrafine particles. Toxicol Pathol. 2018;46(1):75–84. [PubMed: 28914166]
33. Selvaraj K, Gowthamarajan K, Karri V. Nose to brain transport pathways an overview: potential of nanostructured lipid carriers in nose to brain targeting. Artif Cells Nanomed Biotechnol. 2018;46(8):2088–2095. [PubMed: 29282995]
34. Oberdorster G, Elder A, Rinderknecht A. Nanoparticles and the brain: cause for concern? J Nanosci Nanotechnol. 2009;9(8):4996–5007. [PubMed: 19928180]
35. Lucchini RG, Dorman DC, Elder A, Veronesi B. Neurological impacts from inhalation of pollutants and the nose-brain connection. Neurotoxicology. 2012;33(4):838–841. [PubMed: 22178536]
36. Serralheiro A, Alves G, Sousa J, Fortuna A, Falcão A. Nose as a route for drug delivery. In: Önerci T, ed. Nasal Physiology and Pathophysiology of Nasal Disorders. Berlin, Germany: Springer; 2013:191–215.
37. Erdo F, Bors LA, Farkas D, Bajza A, Gizurarson S. Evaluation of intranasal delivery route of drug administration for brain targeting. Brain Res Bull. 2018;143:155–170. [PubMed: 30449731]
38. Potter SM, Zheng C, Koos DS, Feinstein P, Fraser SE, Mombaerts P. Structure and emergence of specific olfactory glomeruli in the mouse. J Neurosci. 2001;21(24):9713–9723. [PubMed: 11739580]

39. Taurozzi JS, Hackley VA, Wiesner MR. Ultrasonic dispersion of nanoparticles for environmental, health and safety assessment—issues and recommendations. Nanotoxicology. 2011;5(4):711–729. doi:10.3109/17435390.2010.528846. [PubMed: 21073401]
40. Golla D, Chattrakun K, Watanabe K, Taniguchi T, LeRoy BJ, Sandhu A. Optical thickness determination of hexagonal boron nitride flakes. Appl Phys Lett. 2013;102(16):161906.
41. Stenzel O, Hahn J, Röder M, Ehrlich A, Prause S, Richter F. The optical constants of cubic and hexagonal boron nitride thin films and their relation to the bulk optical constants. Phys Status Solidi A. 1996;158(1):281–287.
42. Choi AO, Maysinger D. Intranasal fluoresecent nanocrystals for longitudinal in vivo evaluation of cerebral microlesions. Pharm Nanotechnol. 2013;1:93–104.
43. Choi AO, Neibert KD, Maysinger D. Quantum dots for imaging neural cells in vitro and in vivo. In: Fontes A, Santos BS, eds. Quantum Dots: Applications in Biology, Methods in Molecular Biology. New York: Springer Science + Business Media; 2014:191–206.
44. Westin U, Piras E, Jansson B, et al. Transfer of morphine along the olfactory pathway to the central nervous system after nasal administration to rodents. Eur J Pharm Sci. 2005;24(5):565–573. [PubMed: 15784346]
45. Rao GV, Tinkle S, Weissman DN, et al. Efficacy of a technique for exposing the mouse lung to particles aspirated from the pharynx. J Toxicol Environ Health A. 2003;66(15):1441–1452. [PubMed: 12857634]
46. Aimar P, Meireles M, Sanchez V. A contribution to the translation of retention curves into pore size distributions for sieving membranes. J Membr Sc. 1990;54(3):321–338.
47. Jansson B, Bjork E. Visualization of in vivo olfactory uptake and transfer using fluorescein dextran. J Drug Target. 2002;10(5):379–386. [PubMed: 12442808]
48. Kittel B, Ruehl-Fehlert C, Morawietz G, et al. Revised guides for organ sampling and trimming in rats and mice—part 2: a joint publication of the RITA) and NACAD) groups. Exp Toxicol Pathol. 2004;55(6):413–431. [PubMed: 15384248]
49. Sullivan-Brown J, Bisher ME, Burdine RD. Embedding, serial sectioning and staining of zebrafish embryos using JB-4 resin. Nat Protoc. 2011;6(1):46–55. doi:10.1038/nprot.2010.165. [PubMed: 21212782]
50. Bernhard W, Mottaghian J, Gebert A, Rau GA, von Der Hardt H, Poets CF. Commercial versus native surfactants: surface activity, molecular components, and the effect of calcium. Am J Respir Crit Care Med. 2000;162(4, pt 1):1524–1533. [PubMed: 11029372]
51. Nag K, Keough KM, Morrow MR. Probing perturbation of bovine lung surfactant extracts by albumin using DSC and 2H-NMR. Biophys J. 2006;90(10):3632–3642. [PubMed: 16500977]
52. Gugliotti M, Politi MJ. The role of the gel⇔ liquid-crystalline phase transition in the lung surfactant cycle. Biophys Chem. 2001;89(2–3):243–251. [PubMed: 11254217]
53. Marrink SJ, Risselada J, Mark AE. Simulation of gel phase formation and melting in lipid bilayers using a coarse grained model. Chem Phys Lipids. 2005;135(2):223–244. [PubMed: 15921980]
54. Ramteke S, Chelladurai H. Examining the role of hexagonal boron nitride nanoparticles as an additive in the lubricating oil and studying its application. Proc Inst Mech Eng N J Nanomater Nanoeng Nanosyst. 2020;234(1–2):19–36.
55. Çelik O, Ay N, Göncü Y. Effect of nano hexagonal boron nitride lubricant additives on the friction and wear properties of AISI 4140 steel. Part Sci Technol. 2013;31(5):501–506.
56. Boyle P, Humphrey A, Courtney M, Air Force Academy. Quantifying friction effects of molybdenum disulfide, tungsten disulfide, hexagonal boron nitride, and lubalox as bullet coating. Published 2012. Accessed March 19, 2022. https://apps.dtic.mil/sti/pdfs/ADA568594.pdf.
57. Cohen JM, Beltran-Huarac J, Pyrgiotakis G, Demokritou P. Effective delivery of sonication energy to fast settling and agglomerating nanomaterial suspensions for cellular studies: implications for stability, particle kinetics, dosimetry and toxicity. NanoImpact. 2018;10:81–86. [PubMed: 29479575]
58. Kosaka K, Sawai K, Tanaka C, Imafuji M, Kamei A, Kosaka T. Distinct domanial and lamellar distribution of clustered lipofuscin granules in microglia in the main olfactory bulb of young mice. Neurosci Res. 2009;65(3):286–295. doi:10.1016/j.neures.2009.08.001. [PubMed: 19666062]

59. Amiot CL, Xu S, Liang S, Pan L, Zhao JX. Near-infrared fluorescent materials for sensing of biological targets. Sensors (Basel). 2008;8(5):3082–3105. doi:10.3390/s8053082. [PubMed: 27879867]
60. Frangioni JV. In vivo near-infrared fluorescence imaging. Curr Opin Chem Biol. 2003;7(5):626–634. [PubMed: 14580568]
61. Evans CM, Williams OW, Tuvim MJ, et al. Mucin is produced by clara cells in the proximal airways of antigen-challenged mice. Am J Respir Cell Mol Biol. 2004;31(4):382–394. [PubMed: 15191915]
62. Roberts JR, Mercer RR, Chapman RS, et al. Pulmonary toxicity, distribution, and clearance of intratracheally instilled silicon nanowires in rats. J Nanomater. 2012;2012:398302. doi:10.1155/2012/398302. [PubMed: 26640479]
63. Shvedova AA, Kisin ER, Mercer R, et al. Unusual inflammatory and fibrogenic pulmonary responses to single-walled carbon nanotubes in mice. Am J Physiol Lung Cell Mol Physiol. 2005;289(5):L698–708. [PubMed: 15951334]
64. Drescher D, Orts-Gil G, Laube G, et al. Toxicity of amorphous silica nanoparticles on eukaryotic cell model is determined by particle agglomeration and serum protein adsorption effects. Anal Bioanal Chem. 2011;400(5):1367–1373. [PubMed: 21479547]
65. Jiang J, Oberdörster G, Biswas P. Characterization of size, surface charge, and agglomeration state of nanoparticle dispersions for toxicological studies. J Nanopart Res. 2009;11(1):77–89.
66. Duffin R, Tran L, Brown D, Stone V, Donaldson K. Proinflammogenic effects of low-toxicity and metal nanoparticles in vivo and in vitro: highlighting the role of particle surface area and surface reactivity. Inhal Toxicol. 2007;19(10):849–856. doi:10.1080/08958370701479323. [PubMed: 17687716]
67. Elder A, Gelein R, Silva V, et al. Translocation of inhaled ultrafine manganese oxide particles to the central nervous system. Environ Health Perspect. 2006;114(8):1172–1178. [PubMed: 16882521]
68. Bourganis V, Kammona O, Alexopoulos A, Kiparissides C. Recent advances in carrier mediated nose-to-brain delivery of pharmaceutics. Eur J Pharm Biopharm. 2018;128:337–362. [PubMed: 29733950]
69. Sonvico F, Clementino A, Buttini F, et al. Surface-modified nanocarriers for nose-to-brain delivery: from bioadhesion to targeting. Pharmaceutics. 2018;10(1):34. [PubMed: 29543755]
70. Salem LH, El-Feky GS, Fahmy RH, El Gazayerly ON, Abdelbary A. Coated lipidic nanoparticles as a new strategy for enhancing nose-to-brain delivery of a hydrophilic drug molecule. J Pharm Sci. 2020;109(7):2237–2251. [PubMed: 32320670]
71. Froelich A, Osmałek T, Jadach B, Puri V, Michniak-Kohn B. Microemulsion-based media in nose-to-brain drug delivery. Pharmaceutics. 2021;13(2):201. [PubMed: 33540856]
72. Sato Y, Sano M. Dispersing single-walled carbon nanotubes using common phospholipids with a small amount of polyethylene glycol-phospholipid additives. Colloids Surf A Physicochem Eng Asp. 2014;441:427–432.
73. Li J, Wang X, Zhang T, et al. A review on phospholipids and their main applications in drug delivery systems. Asian J Pharm Sci. 2015;10(2):81–98.
74. Pichot R, Watson RL, Norton IT. Phospholipids at the interface: current trends and challenges. Int J Mol Sci. 2013;14(6):11767–11794. [PubMed: 23736688]
75. Seantier B, Breffa C, Felix O, Decher G. In situ investigations of the formation of mixed supported lipid bilayers close to the phase transition temperature. Nano Letters. 2004;4(1):5–10.
76. Lee A Lipid phase transitions and phase diagrams. I. Lipid phase transitions. Biochim Biophys Acta. 1977;472(2):237–281. [PubMed: 329881]
77. Veldhuizen R, Nag K, Orgeig S, Possmayer F. The role of lipids in pulmonary surfactant. Biochim Biophys Acta. 1998;1408(2–3):90–108. [PubMed: 9813256]
78. Guo Y, Terazzi E, Seemann R, Fleury JB, Baulin VA. Direct proof of spontaneous translocation of lipid-covered hydrophobic nanoparticles through a phospholipid bilayer. Sci Adv. 2016;2(11):e1600261. [PubMed: 27847863]

79. Oosterlaken-Dijksterhuis MA, Haagsman HP, Van Golde LM, Demel RA. Interaction of lipid vesicles with monomolecular layers containing lung surfactant proteins SP-B or SP-C. Biochemistry. 1991;30(33):8276–8281. [PubMed: 1868098]
80. Oosterlaken-Dijksterhuis MA, Haagsman HP, Van Golde LM, Demel RA. Characterization of lipid insertion into monomolecular layers mediated by lung surfactant proteins SP-B and SP-C. Biochemistry. 1991;30(45):10965–10971. [PubMed: 1932022]
81. Shiffer K, Hawgood S, Duzgunes N, Goerke J. Interactions of the low molecular weight group of surfactant-associated proteins (SP 5–18) with pulmonary surfactant lipids. Biochemistry. 1988;27(8):2689–2695. [PubMed: 3401444]
82. Poulain FR, Nir S, Hawgood S. Kinetics of phospholipid membrane fusion induced by surfactant apoproteins A and B. Biochim Biophys Acta. 1996;1278(2):169–175. [PubMed: 8593273]
83. Wang H, Shang L, Maffre P, et al. The nature of a hard protein corona forming on quantum dots exposed to human blood serum. Small. 2016;12(42):5836–5844. doi:10.1002/smll.201602283. [PubMed: 27606563]
84. Evans TW. Review article: albumin as a drug—biological effects of albumin unrelated to oncotic pressure. Aliment Pharmacol Ther. 2002;16(suppl 5):6–11. [PubMed: 12423448]
85. Labelle P, Hahn NE, Fraser JK, et al. Mousepox detected in a research facility: case report and failure of mouse antibody production testing to identify Ectromelia virus in contaminated mouse serum. Comp Med. 2009;59(2):180–186. [PubMed: 19389311]
86. Soll RF, Hoekstra RE, Fangman JJ, et al. Multicenter trial of single-dose modified bovine surfactant extract (Survanta) for prevention of respiratory distress syndrome. Pediatrics. 1990;85(6):1092–1102. [PubMed: 2187176]
87. Adamkin D, McClead RE Jr, Desai NS, McCulloch KM, Marchildon MB. Comparison of two neonatal intravenous amino acid formulations in preterm infants: a multicenter study. J Perinatol. 1991;11(4):375–382. [PubMed: 1770397]
88. American Society for Testing and Materials. Standard Guide for Measurement of Particle Size Distribution of Nanomaterials in Suspension by Photon Correlation Spectroscopy (PCS)(E2490–09). West Conshohocken, PA: ASTM International; 2015.
89. Kokkinopoulou M, Simon J, Landfester K, Mailänder V, Lieberwirth I. Visualization of the protein corona: towards a biomolecular understanding of nanoparticle-cell-interactions. Nanoscale. 2017;9(25):8858–8870. [PubMed: 28632260]
90. Arenas-Guerrero P, Delgado AV, Donovan KJ, et al. Determination of the size distribution of non-spherical nanoparticles by electric birefringence-based methods. Sci Rep. 2018;8(1):9502. doi:10.1038/s41598-018-27840-0. [PubMed: 29934624]
91. Liu T, Xiao Z. Dynamic light scattering of rigid rods: a universal relationship on the apparent diffusion coefficient as revealed by numerical studies and its use for rod length determination. Macromol Chem Phys. 2012;213(16):1697–1705.
92. Au WW, Treloar HB, Greer CA. Sublaminar organization of the mouse olfactory bulb nerve layer. J Comp Neurol. 2002;446(1):68–80. [PubMed: 11920721]

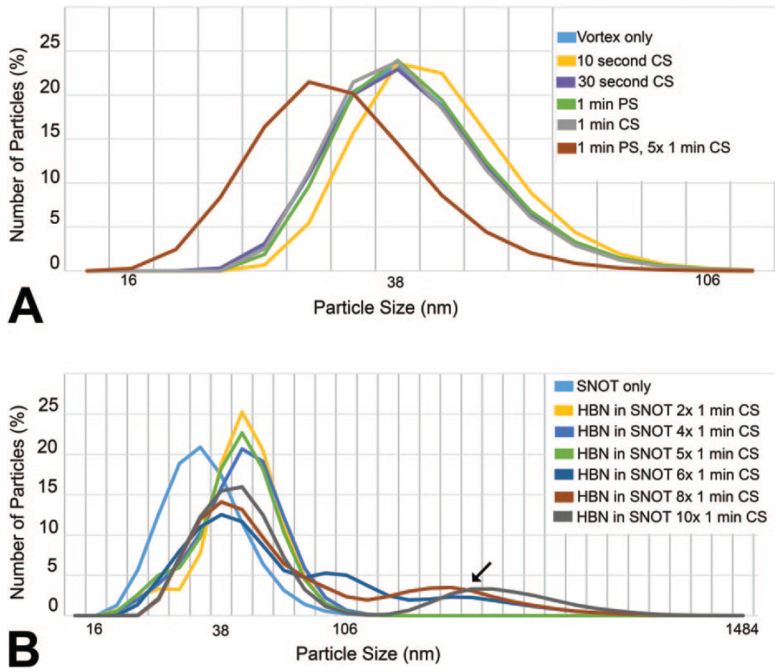

Figure 1.

The effect of variations in vortexing and sonication procedures on the diameter of particles measured by dynamic light scattering (DLS) in solutions of (A) SNOT alone or (B) HBN dispersed in SNOT. As shown in A, vortexing and either cup sonication (CS) or probe sonication (PS) produced similar particle (vesicle) diameter for SNOT itself and the particle size distributions frequently overlapped for vortexing and sonication times of 30 seconds to 1 minute. SNOT vesicles were slightly larger with a 10-second sonication and were smaller with repeated sonication. As shown in B, the particle size of HBN in SNOT was slightly larger than for SNOT alone. With six or more CSs a population of particles of larger dimensions was noted (arrow). HBN indicates hexagonal boron nitride; SNOT, solution for nasal and olfactory transport.

Figure 2.
Polarized light microscopy of hexagonal boron nitride (HBN) (0.18 mg/mL) dispersed in SNOT. HBN polarizes light, enabling confirmation of well-dispersed HBN preparations. Bar = 12 microns.

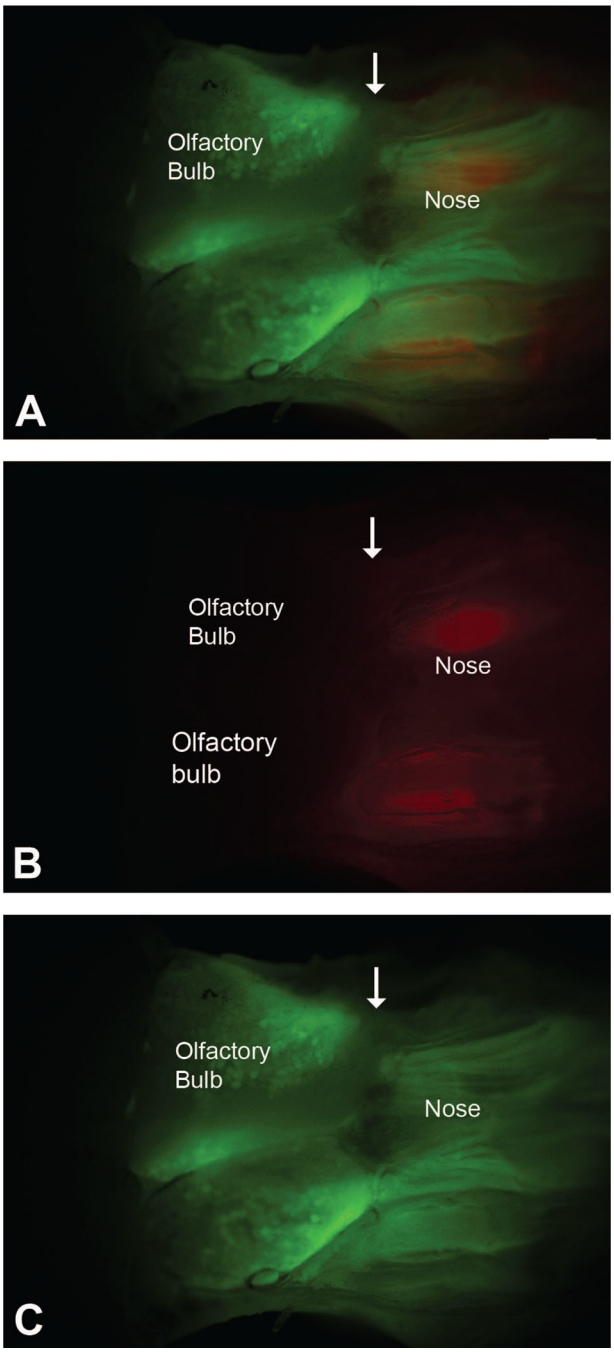

Figure 3.

Epifluorescence stereomicroscopy demonstrates red dextran dye (3000 MW anionic lysine-fixable tetramethylrhodamine dextran) at a 0.5% concentration in SNOT following intranasal instillation reached the olfactory region of the nose, although passage beyond the location of the cribriform plate (arrow) was difficult to demonstrate. (A) Dual label stereomicroscopy with the dextran dye in red and the olfactory neurons in green. (B) Red fluorescence shows the location of the red dextran dye. (C) Green fluorescence from GFP expression in the olfactory neurons of the B6;129P2-Omp^{tm3Mom}/MomJ heterozygous mouse shows the

location of olfactory neurons which have the cell body in the nose with axons that traverse the cribriform plate to enter the olfactory bulb of the brain. GFP indicates green fluorescence protein; SNOT, solution for nasal and olfactory transport.

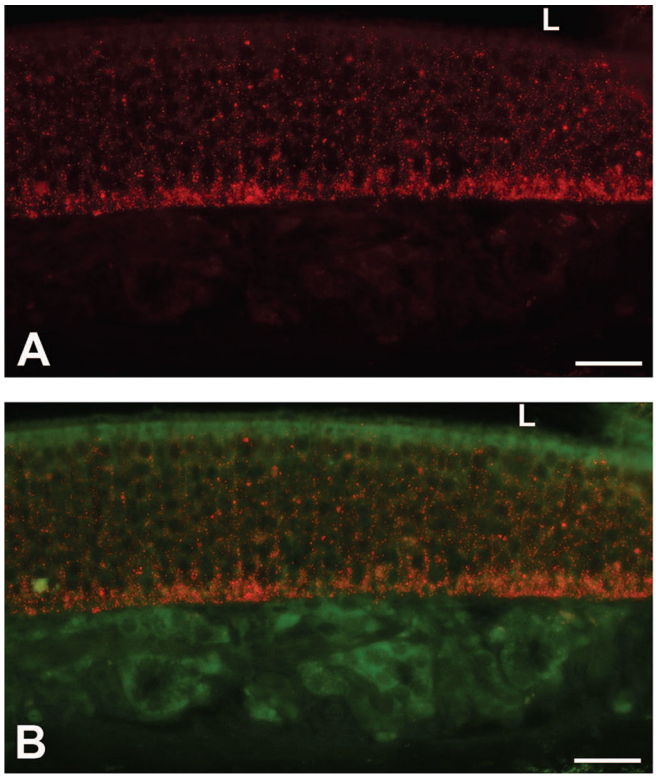

Figure 4.

Fluorescence imaging of unstained plastic sections at level T2 of the nose 1 day after exposure demonstrate red fluorescence consistent with uptake of lysine-fixable rhodamine dextran dispersed in SNOT in exposed mice. (A) This focus contains punctate red fluorescent material consistent with the rhodamine dextran dye extending from near the lumen (L) at the top of the photomicrograph to the basement membrane. (B) The same focus with green autofluorescence superimposed on the red fluorescent material demonstrates that the punctate material is within the neuroepithelium of the nose. Bar = 25 microns.

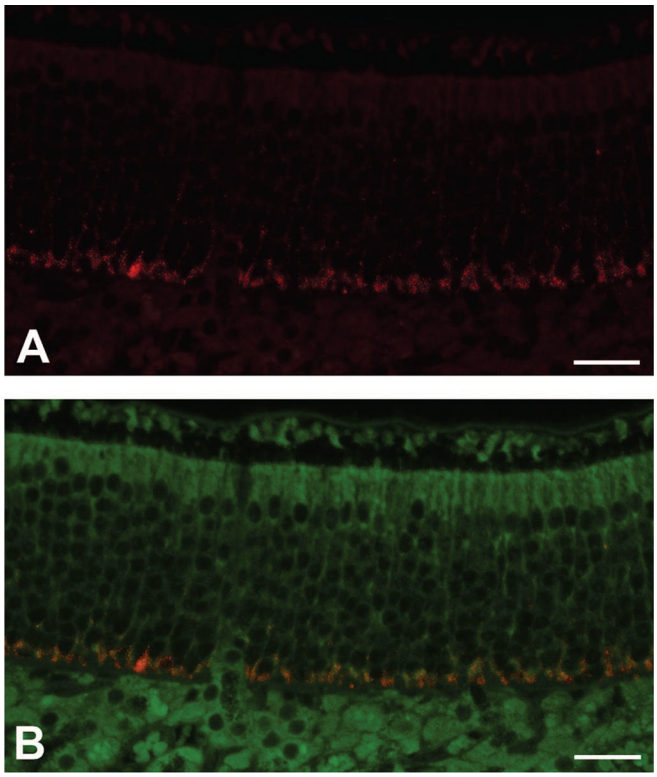

Figure 5.

Fluorescence imaging of an unstained plastic section at level T2 of the nose 1 week after exposure demonstrates red fluorescence consistent with uptake of lysine-fixable rhodamine dextran dispersed in solution for nasal and olfactory transport in exposed mice. (A) This focus contains punctate red fluorescent material consistent with the rhodamine dextran dye that is localized in a linear band near the basement membrane. (B) The same focus with green autofluorescence superimposed on the red fluorescent material demonstrates that the punctate material is located near the basement membrane of the neuroepithelium at the site of the basal cells. Reference bar = 25 microns.

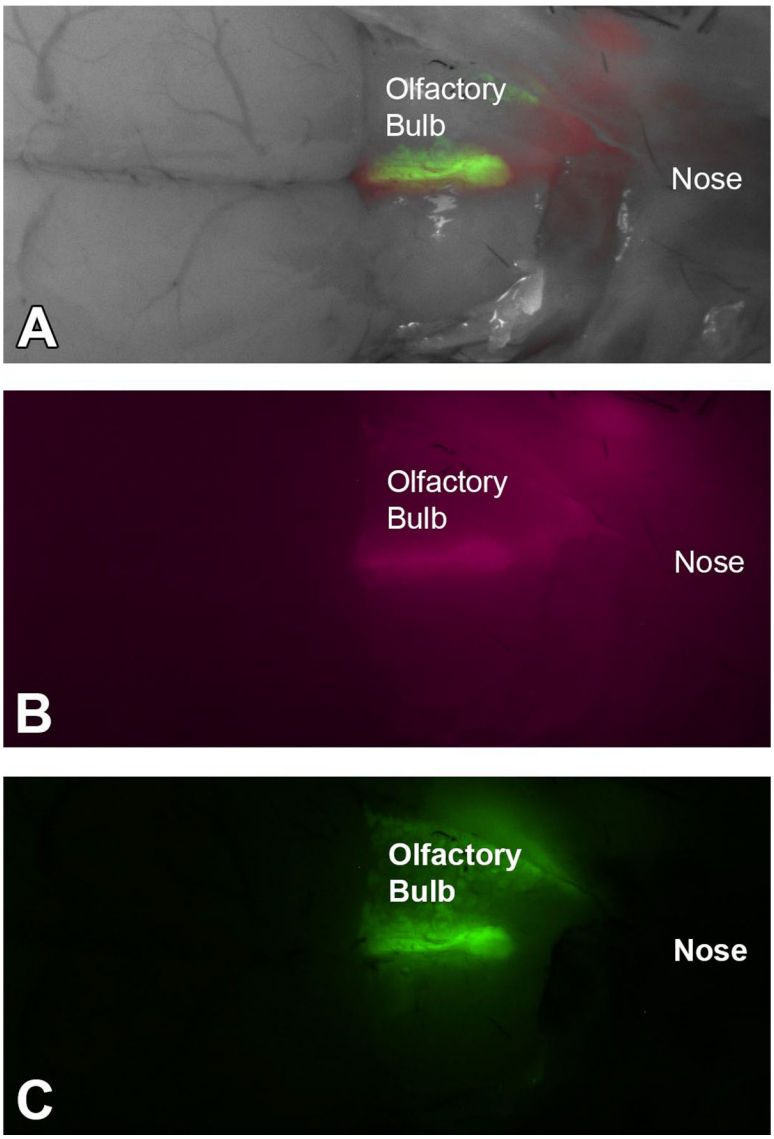

Figure 6.

Stereomicroscopic image showing near-infrared (NIR) dextran in SNOT reaching the GFP-positive, green fluorescent axons of olfactory neurons that are in the olfactory nerve fibers and the glomeruli of the olfactory bulb of the GFP-OMP mouse. (A) Stereomicroscopic image of the nose, olfactory bulb, and cerebrum with superimposed green and NIR epifluorescence stereomicroscopy demonstrating that the NIR-dextran frequently co-localizes with olfactory neurons. (B) NIR fluorescence showing the location of the NIR dextran. (C) Green fluorescence from GFP expression in the axons of the olfactory neurons of the B6;129P2-*Omp*^{tm3Mom}/MomJ heterozygous mouse. The spherical pale green structures are the glomeruli of the olfactory bulb where the first neuronal synapse occurs in the olfactory bulb. The more intense green linear structures are consistent with olfactory nerve fibers. GFP indicates green fluorescence protein; OMP, olfactory marker protein gene; SNOT, solution for nasal and olfactory transport.

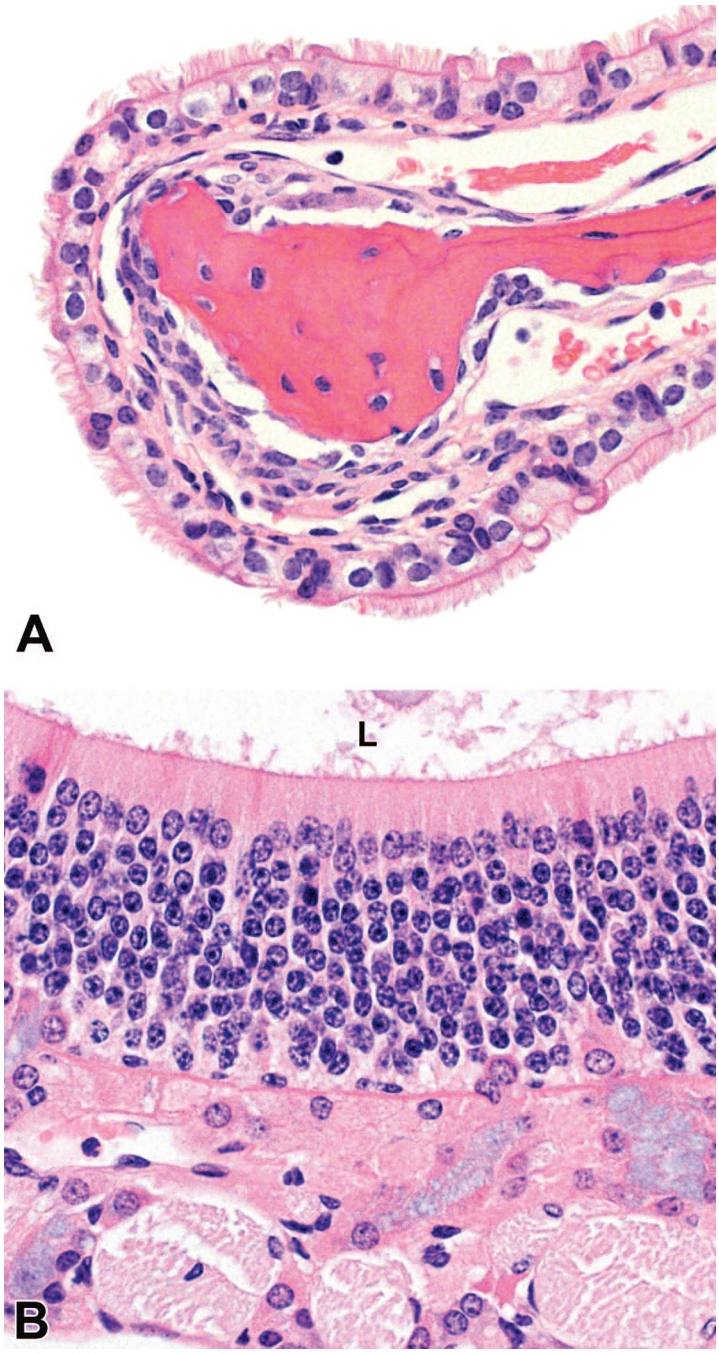

Figure 7.

Intranasal instillation of solution for nasal and olfactory transport did not cause changes in nasal morphology. (A) Normal maxilloturbinate and (B) normal olfactory neuroepithelium are representative of the normal nasal morphology in a mouse intranasally instilled with SNOT 1 hour prior to necropsy. The lumen (L) is at the top of the photomicrograph in B.

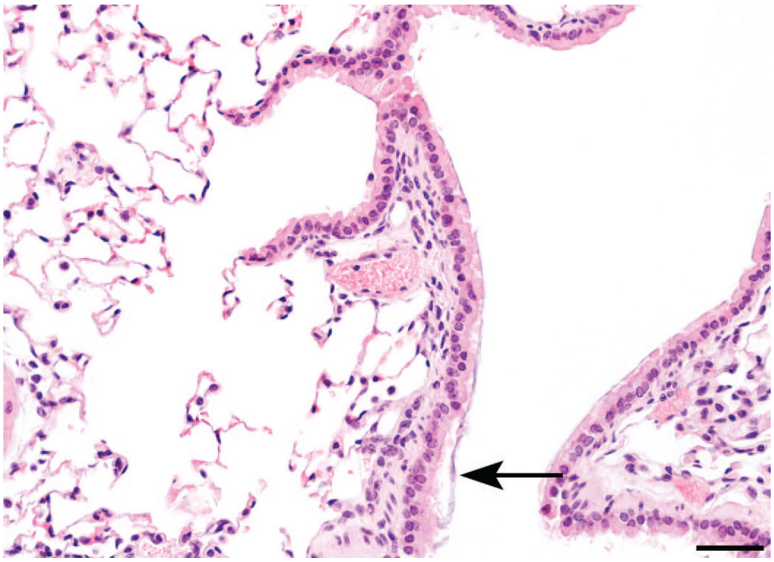

Figure 8.

Lung of a mouse 1 day after pharyngeal aspiration of SNOT. A slightly basophilic film morphologically consistent with mucus or potentially with retained SNOT lines the second-generation bronchiole of this mouse (arrow). Bar = 50 microns.

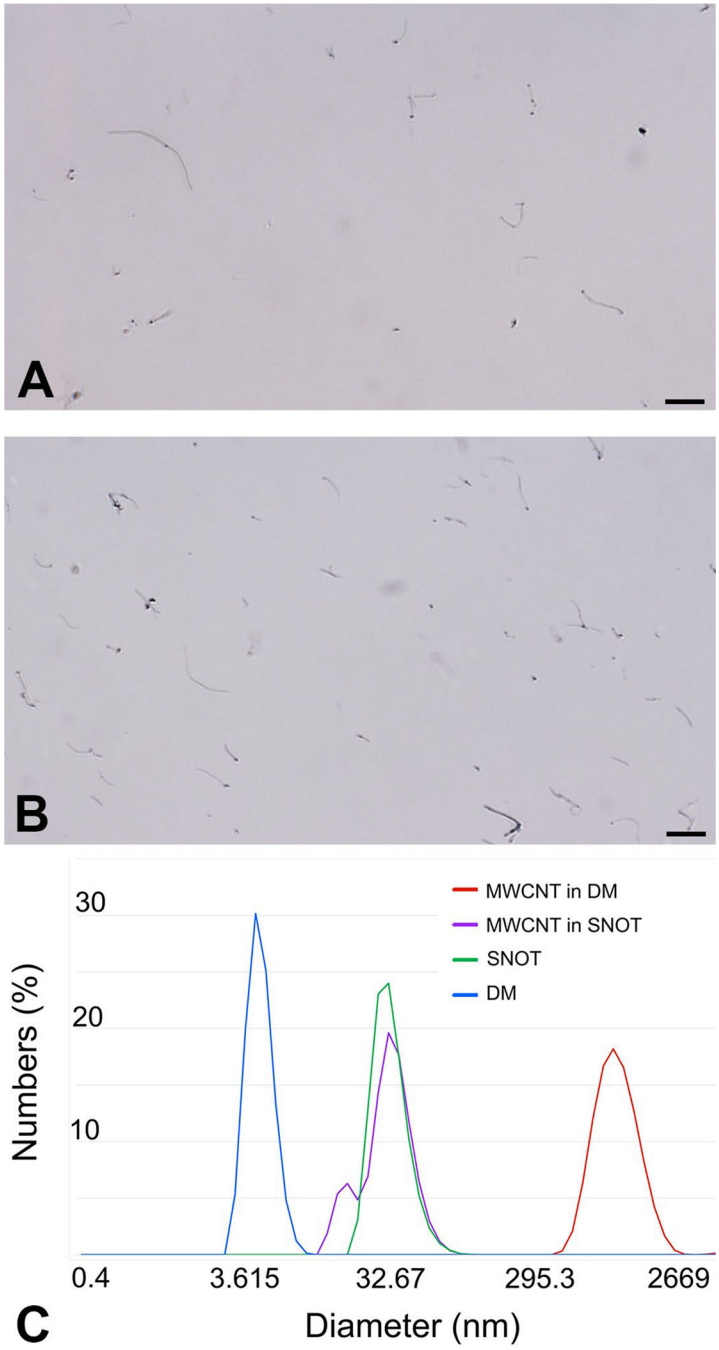

Figure 9.

MWCNTs dispersed in DM and then diluted in SNOT are well-dispersed and their size measured by DLS is less than the size of MWCNTs in DM. (A) Light microscopic image showing well-dispersed MWCNT in DM at 0.1 mg/mL. (B) Light microscopic image showing well-dispersed MWCNT in a SNOT solution containing 89.5% SNOT and 10.5% DM. (C) DLS of SNOT, DM, MWCNT in DM (0.1 mg/mL), and MWCNT first dispersed in DM at a 0.95 mg/mL and then diluted in SNOT to produce a concentration of 0.1 mg/mL of MWCNT (actual concentration 89.5% SNOT and 10.5% DM). DLS measures particles not

visible to the human eye in each solution and measures a smaller size for MWCNT in SNOT solution than in DM. The change in DLS-detected size may be relative rather than a specific size change since a limitation of using DLS for measuring the size of fiber-like particles is that the size calculated by DLS is based upon light-scattering by spherical particles. Bar = 10 microns. DLS indicates dynamic light scattering; DM, dispersion media; MWCNTs, multiwalled carbon nanotubes; SNOT, solution for nasal and olfactory transport.

Table 1.

Parameters for measurement via DLS.

Sample	Hydrodynamic diameter	Unit	Temperature (°C)
HBN			
Material refractive index	1.800	Unitless	N/A
Material absorbance	0.010	Au	N/A
SNOT			
Density	1.01039	g/mL	37
Refractive index	1.336	Unitless	37
Dynamic viscosity	0.8037	cP	37

Abbreviations: DLS, dynamic light scattering; HBN, hexagonal boron nitride; SNOT, solution for nasal and olfactory transport.

Table 2.

Estimated median hydrodynamic diameter (nm) of SNOT alone determined from DLS and statistics from Figure 1A.

Sample	Median	95% CI		IQR[a]
		LB	UB	
Vortex only	40.8	38.2	43.8	18.1
10-second CS	43.8	40.8	45.7	12.9
30-second CS	40.8	38.2	43.5	18.1
1-minute PS	40.8	38.2	43.8	18.1
1-minute CS	40.8	38.2	43.5	14.6
1-minute PS, 5 × 1-minute CS	32.4	30.4	34.1	13.5

Three replicates were done on three consecutive days and the median was calculated for all nine of those values. The PDI was less than 0.3 for all samples. Abbreviations: CI, confidence intervals; CS, cup sonication; DLS, dynamic light scattering; IQR, interquartile range; LB, lower bounds; PDI, polydispersity index; PS, probe sonication; SNOT, solution for nasal and olfactory transport; UB, upper bounds.

[a] IQR value could not be interpolated between diameter points.

Table 3.

Estimated median hydrodynamic diameter (nm) of HBN in SNOT from DLS measurements and statistics from Figure 1B.

Sample	PDI	Median	95% CI		IQR[a]
			LB	UB	
SNOT only	0.179	35.3	32.7	37.6	15.6
2× sonication	0.523	44.3	41.7	47.3	12.9
4× sonication	0.500	44.3	41.7	47.3	12.9
5× sonication	0.506	43.8	40.8	46.2	12.9
6× sonication	0.475	48.1	41.7	55.7	35.4
8× sonication	0.524	45.7	41.7	51.3	26.1
10× sonication	0.488	43.5	40.8	45.7	18.1

IQR value could not be interpolated between diameter points.

Abbreviations: CI, confidence intervals; DLS, dynamic light scattering; HBN, hexagonal boron nitride; IQR, interquartile range; LB, lower bounds; PDI, polydispersity index; SNOT, solution for nasal and olfactory transport; UB, upper bounds.

[a]Values represent three replicates done on each of five consecutive days (15 replicates total). The median represents the calculated median from each of the 15 measurements.

Table 4.

Number of mice examined and showing strong (or equivocal) red fluorescence in the nose and olfactory bulb by stereomicroscopy epifluorescence after intranasal instillation of rhodamine dextran or SNOT alone during the rhodamine dextran time course experiment.

Sample	Time post exposure	Number examined	Nose negative	Nose positive (faint positive)[a]	Olfactory bulb negative	Olfactory bulb positive (faint positive)[a]
0.5% rhodamine dextran[b]	3 hours	3	0	3 (0)	3	0 (0)
0.5% rhodamine dextran[b]	6 hours	3	0	3 (0)	2	0 (1)
0.5% rhodamine dextran[b]	1 day	3	0	0 (3)	3	0 (0)
0.5% rhodamine dextran[b]	1 week	3	3	0 (0)	3	0 (0)
SNOT	3 hours	3	3	0 (0)	3	0 (0)
SNOT	1 week	3	3	0 (0)	3	0 (0)

Abbreviation: SNOT, solution for nasal and olfactory transport.

[a]Positive was scored when strong fluorescence was emitted from the tissue of interest when viewed using the red fluorescence light source. A few mice showed faint or equivocal red fluorescence not seen in the SNOT controls and those were not scored as positive but are noted in parentheses.

[b]0.5% Tetramethylrhodamine 3000 MW anionic lysine-fixable dextran in SNOT.

Table 5.

Number of mice examined and showing strong (or equivocal) fluorescence in the nose and olfactory bulb by stereomicroscopy epifluorescence after intranasal instillation of NIR dextran in SNOT or SNOT alone.

Sample	Time post exposure	Number examined	Nose negative	Nose positive (faint positive)[a]	Olfactory bulb negative	Olfactory bulb positive (faint positive)[a]
0.5% NIR dextran[b]	15 minutes	2	0	2 (0)	0	2 (0)
0.5% NIR dextran[b]	30 minutes	3	0	3	0	3 (0)
0.5% NIR dextran[b]	1 hour	2	0	2 (0)	0	1 (1)
0.5% NIR dextran[b]	6 hours	3	0	3 (0)	0	2 (1)
0.5% NIR dextran[b]	1 day	3	0	1 (2)	2	1 (0)
SNOT	All time points[c]	14	14	0 (0)	14	0 (0)

Abbreviations: NIR, near-infrared; SNOT, solution for nasal and olfactory transport.

[a]Positive was scored when distinct fluorescence was emitted from the tissue of interest when viewed using the NIR excitation. A few mice showed faint or equivocal NIR fluorescence not seen in the SNOT controls and those were not scored as positive but were noted in parentheses.

[b]Alexa Fluor 680 3000 MW anionic dextran.

[c]SNOT-exposed mice were evaluated at 15 minutes (n = 3), 30 minutes (n = 2), 1 hour (n = 3), 6 hours (n = 3), and 1 day (n = 3).

Table 6.

Number of mice evaluated for histopathologic alterations in routine paraffin-embedded H&E-stained sections of nose.

	Time after exposure			
Sample	**1 hour**	**3 hours**	**6 hours**	**1 day**
SNOT	3	1	3	3
0.5% rhodamine dextran[a]	3	1	1	ND
0.5% NIR dextran[b]	ND	ND	3	3

A minimum of three levels were evaluated from each mouse. Four levels of nose were trimmed from each mouse in the study. No exposure-related alterations were present in any mouse exposed to SNOT or a dextran dye in SNOT. Artifactual tissue tears and tissue debris attributable to the removal of the neurocalvarium were seen in some tissue sections where the nose and brain were examined by stereomicroscopy. In some mice, T2 level of the nose was processed for plastic sections, resulting in only three levels (T1, T3, and T4) being paraffin-embedded and evaluated in H&E sections from those mice.

Abbreviations: ND, not done; NIR, near-infrared; SNOT, solution for nasal and olfactory transport.

[a]0.5% Tetramethylrhodamine 3000 MW anionic lysine-fixable dextran in SNOT.

[b]Alexa Fluor 680 3000 MW anionic dextran.